Nanoscale

PAPER

View Article Online
View Journal | View Issue

Cite this: *Nanoscale*, 2019, **11**, 20777

Frustrated Lewis pairs photocatalyst for visible light-driven reduction of CO to multi-carbon chemicals†

Zhe Chen,[a,b] Jia Zhao,[b] Jingxiang Zhao, *[b] Zhongfang Chen *[c] and Lichang Yin *[a]

Received 2nd September 2019,
Accepted 9th October 2019

DOI: 10.1039/c9nr07559c

rsc.li/nanoscale

Photocatalytic reduction of carbon monoxide (CO), an increasingly available and low-cost feedstock that could benefit from CO_2 reduction, to high value-added multi-carbon chemicals, is significant for desirable carbon cycling, as well as high efficiency conversion and high density storage of solar energy. However, developing low cost but highly active photocatalysts with long-term stability for CO coupling and reduction remains a great challenge. Herein, by density functional theory (DFT) computations and taking advantage of the frustrated Lewis pairs (FLPs) concept, we identified a complex consisting of single boron (B) atom decorated on the optically active C_2N monolayer (*i.e.*, B/C_2N) as an efficient and stable photocatalyst for CO reduction. On the designed B/C_2N catalyst, CO can be efficiently reduced to ethylene (C_2H_4) and propylene (C_3H_6) both with a free energy increase of 0.22 eV for the potential-determining step, which greatly benefits from the pull–push function of the B–N FLPs composed of the decorating B atom and host N atoms. Moreover, the newly designed B/C_2N catalyst shows significant visible light absorption with a suitable band position for CO reduction to C_2H_4 and C_3H_6. All these unique features make the B/C_2N photocatalyst an ideal candidate for visible light driven CO reduction to high value-added multi-carbon fuels and chemicals.

1. Introduction

The reduction of carbon dioxide (CO_2) to other carbon-based feedstocks and fuels has been considered as a promising solution to cope with the growing greenhouse effect and energy crisis. To date, numerous catalysts for CO_2 reduction, such as metals, metal alloys and oxides (*e.g.*, Au, Ag, and Pd nanoparticles, Cu–Pd and Au–Cu alloys, Cu_2O, and SnO_2),[1–12] 2D metal dichalcogenides (*e.g.*, MoS_2 and WSe_2),[13,14] metal–organic frameworks (MOFs),[15,16] covalent organic frameworks (COF),[17] and N-doped carbon materials,[18–21] have been developed. Remarkably, by CO_2 reduction, C_1 products such as carbon monoxide (CO) and formate ($HCOO^-$) can be produced with high efficiency and high selectivity (*i.e.*, faradaic efficiency) at a low energy cost. However, high value-added multi-carbon chemicals, namely, C_n ($n \geq 2$), have been rarely harvested due to the large overpotential and low selectivity for C–C coupling.[22–26] Thus, to achieve an effective and sustainable carbon-cycle utilization, further reducing C_1 products to high value-added C_n chemicals with high efficiency is an alternative strategy for direct reduction of CO_2 to C_n chemicals.[23,27–29]

Note that CO is one of the key intermediates for C–C coupling during the reduction of CO_2 to C_n products.[27,28] Directly using high pressure CO as the initial reactant has great advantages to promote the C–C coupling. In addition, CO reduction can be carried out in an alkaline electrolyte without producing undesirable carbonate, which can also inhibit the competitive hydrogen evolution reaction, thus enhancing the productivity of C_n chemicals.[23] Therefore, it is of great economic and scientific importance to develop new catalysts with high efficiency and selectivity but low energy consumption to reduce CO to C_n chemicals based on C–C coupling.

Recently, the metal-free frustrated Lewis pairs (FLPs) comprised of a sterically encumbered donor and acceptor, for examples, intra- or inter-molecular B–P, B–N and B–B atomic pairs, have been demonstrated to be effective for the activation of many small molecules, such as H_2, CO, CO_2, NO, SO_2 and

[a]*Shenyang National Laboratory for Materials Science, Institute of Metal Research, Chinese Academy of Sciences, Shenyang, 110016, China. E-mail: lcyin@imr.ac.cn*
[b]*College of Chemistry and Chemical Engineering, and Key Laboratory of Photonic and Electronic Bandgap Materials, Ministry of Education, Harbin Normal University, Harbin, 150025, China. E-mail: xjz_hmily@163.com*
[c]*Department of Chemistry, University of Puerto Rico, Rio Piedras Campus, San Juan, PR, 00931, USA. E-mail: zhongfangchen@gmail.com*
†Electronic supplementary information (ESI) available. See DOI: 10.1039/c9nr07559c

so on.[30–35] In particular, the B species in the FLPs shows strong potential to capture and activate CO, in which B species accepts electrons from CO by σ donation and simultaneously donates electrons from its filled p orbital to the π* orbital of CO, thus weakening the C≡O triple bond. This resembles the widely reported transition metal-CO and B-N_2 interactions.[36–40,53] Therefore, we speculate that the FLPs with B and N dual active sites might be effective at facilitating the C–C coupling during the CO reduction to C_n chemicals, in which the B site acts as a Lewis acid to strongly capture one CO molecule,[39,40] while the N site serves as a Lewis base to push another CO molecule to couple with the first CO. From this point of view, we have constructed a metal-free catalyst for CO reduction, namely, single boron (B) atom decorated on monolayer C_2N (*i.e.*, B/C_2N), which has been widely adopted as the substrate for single atom deposition due to its two-dimensional (2D) structure with uniformly distributed cavities, as well as pyridine-like host N atoms as coordination sites.[41–43] The decorating B atom and host N atoms of monolayer B/C_2N may form intra-molecular B–N FLPs with the pull–push function, thus promoting the CO coupling and facilitating the CO reduction to C_n chemicals.

In this work, by means of density functional theory (DFT) computations, we firstly evaluated the structural stability of the B/C_2N complex based on *ab initio* molecular dynamics (AIMD) simulations and phonon spectrum calculations, confirmed the existence of B–N FLPs, and then explored its catalytic role in promoting multi-CO coupling and reduction. Our DFT results show that CO can be efficiently reduced to ethylene (C_2H_4) and propylene (C_3H_6) on B/C_2N both with a rather low free energy barrier (0.22 eV) for the potential-determining step under visible light irradiation due to the presence of B–N FLPs. This study not only has identified a highly efficient metal-free photocatalyst for CO reduction to high value-added C_n chemicals but also may guide the future development of photo/electrochemical catalysts with high efficiency and selectivity.

2. Results and discussion

Stability of the B/C_2N monolayer with B–N FLPs

Before exploring its possible catalytic role in CO reduction, we examined the structural stability of our designed B/C_2N in order to evaluate its experimental feasibility, which is the prerequisite for practical applications of newly designed catalysts with long-term activity. In the case of monolayer C_2N, there are five possible sites for the decoration of an isolated B atom, and thus we investigated the stabilities of all these five B/C_2N complexes (Fig. 1 and Table S1 in the ESI†).

Among these five possible decoration sites, we found that the corner (site 2 in Fig. 1) of the six-fold cavity is energetically the most favorable site for anchoring an isolated B atom (with an adsorption energy of −5.46 eV), and the resultant B/C_2N complex is featured by a $N_2C_2B_1$ five-membered ring. Such a strong binding (−5.46 eV) implies a high possibility to experimentally achieve this B/C_2N complex containing $N_2C_2B_1$ five-membered rings.

As shown in Fig. 1, except for the two N atoms which form the $N_2C_2B_1$ five-membered ring after B atom decoration, the remaining four N atoms in the cavity of C_2N have large distances (3.1 and 4.2 Å) from the decorating B atom. Such large B–N distances can effectively avoid the quenching of electron donors and acceptors, thus making it possible to form the B–N FLPs in this case.

We further evaluated the thermal stability of this B/C_2N complex by the AIMD simulations at 500 K and 1000 K for 10 ps with a time step of 2 fs (Fig. S1 in the ESI†). For both cases, the energy of the B/C_2N complex oscillates near the equilibrium state, and the atomic structure remains intact without obvious structure distortion during the 10 ps AIMD simulation period, indicating its high thermodynamic stability. We also confirmed that this B/C_2N monolayer is dynamically stable, as no imaginary modes were observed in the phonon dispersion spectrum (Fig. S2 in the ESI†).

All the above results and analyses have confirmed that this lowest-energy structure of B/C_2N monolayer (see Fig. 1, the right panel) has a high stability featuring possible B–N FLPs. Thus, in the following sections, this model was adopted to examine the catalytic performance of the B/C_2N monolayer for CO reduction.

Catalytic activity of B/C_2N towards CO reduction

As is well known, the stable adsorption of multiple CO molecules at the catalytic active site is critical for multi-CO coupling

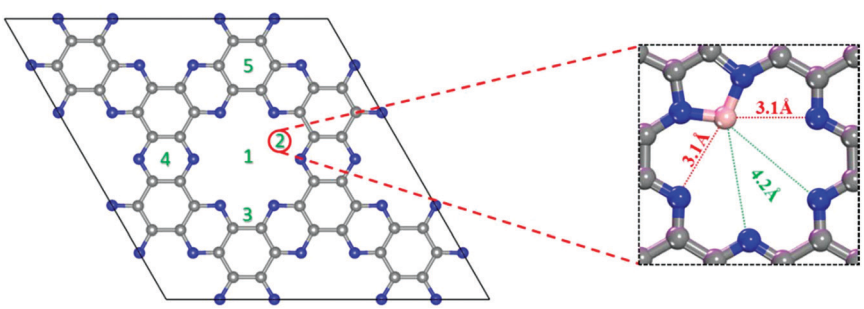

Fig. 1 Schematic structures of the pristine C_2N layer with five possible sites for atomic B decoration. The most stable structure is enlarged and highlighted on the right panel. The relevant B–N distances are also given.

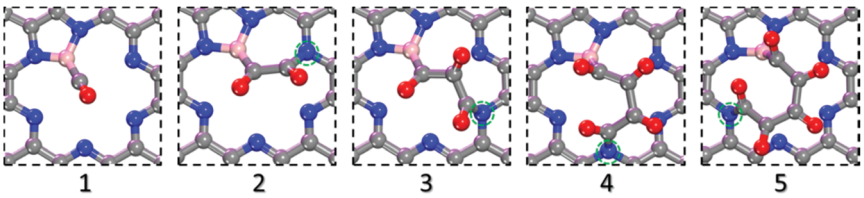

Fig. 2 Schematic diagrams of one to five CO molecules adsorbed on B/C_2N. The C, N, B and O atoms are denoted by gray, blue, pink and red balls, respectively. The host N atoms (N_{CO}) directly binding with the adsorbed CO are highlighted by the green dashed circles.

and subsequent CO reduction to C_n products.[25,44–46] Fig. 2 illustrates the fully optimized structures for the adsorption of one to five CO molecules on B/C_2N, and Table 1 summarizes the corresponding adsorption energies and adsorption free energies. The adsorption energy of a single CO molecule on B/C_2N is −2.41 eV, due to a strong capture ability of the decorated B atom for the CO molecule. As the number of adsorbed CO molecules increases, each newly introduced CO molecule is linked with the former one by C–C coupling, giving rise to a gradually prolonged carbon skeleton (see Fig. 2). During this process, the carbon skeleton is well supported together by the decorated B atom and host N atoms of the B/C_2N complex. Meanwhile, the calculated adsorption energy (ranging from −2.85 to −3.02 eV) of multi-CO on B/C_2N does not change too much upon increasing the number of CO molecules from two to five (see Table 1). After considering the contribution of zero-point energy and entropy, the calculated adsorption free energies of CO on B/C_2N gradually increase (*i.e.*, less favorable) upon increasing the number of adsorbed CO molecules.

Note that all the calculated adsorption free energies of two, three and four CO molecules on B/C_2N are negative, indicating that the multi-CO coupling is thermodynamically spontaneous for these three cases. As for the 5th CO adsorption, a positive but still moderate adsorption free energy (0.58 eV) is obtained. In this case, we believe that the multi-CO coupling for the 5th CO adsorption may also occur by increasing the concentration of gaseous CO at somewhat energy cost. Therefore, we speculate that different C_n chemicals including C_2, C_3, C_4, and even C_5 can be produced by CO reduction on B/C_2N. Considering the extremely complex and overlong reaction path of CO reduction to C_4 and C_5 chemicals, we only take C_2 and C_3 as examples of possible C_n products from CO reduction to evaluate the catalytic performance of B/C_2N in this work.

For the C–C coupling process, in addition to the thermodynamics as we discussed above, kinetics is the other important issue. Thus, we studied the detailed reaction pathway for C–C coupling by the climbing image nudged elastic band (CI-NEB) method. Starting from the barrier-free chemisorption of the 1st CO molecule on B/C_2N, we sequentially calculated the energy barriers from physisorption to chemisorption (C–C coupling) for the 2nd and the 3rd CO molecule. As shown in Fig. 3, when the 2nd CO approaches and bonds with the 1st pre-chemisorbed *CO on B/C_2N to form *COCO, a moderate energy barrier of 0.73 eV is observed with an energy decrease of 0.31 eV. When introducing the 3rd CO, the formation of *COCOCO leads to a negligible energy release (0.01 eV), and the calculated energy barrier from *COCO + CO to *COCOCO is 0.83 eV. The moderate energy barriers (0.73 and 0.83 eV) for these two C–C coupling processes (*CO + CO to *COCO and *COCO + CO to *COCOCO) on B/C_2N are comparable with those (about 0.48 and 0.90 eV) at the interface of between Cu (111) and Cu (100); both have been demonstrated to be able to reduce CO to *n*-propanol with a 20% faradaic efficiency at a low potential of −0.45 V *versus* the reversible hydrogen electrode.[28]

The above results clearly show that the C–C coupling is energetically favorable and occurs spontaneously for the adsorption of up to three CO molecules on B/C_2N, probably due to the existence of the B–N FLPs in our designed B/C_2N complex and its catalytic role in C–C coupling. To verify this speculation, we further calculated the difference charge density of B/C_2N with two adsorbed CO molecules. As shown in Fig. S3a and 3b in the ESI,† the charge accumulation occurs between the decorating B atom and the C atom of the first CO, while charge depletion appears between the host N atom and the C atom of the second CO. Furthermore, when considering the multi-CO (one to five CO molecules) adsorption, the dec-

Table 1 The calculated adsorption energies (E_{ad}) and adsorption free energies (G^*_{ad}) of one to five CO molecules on B/C_2N

Numbers of CO	E_{ad} (eV)	G^*_{ad} (eV)
1	−2.41	−1.72
2	−2.85	−1.39
3	−2.98	−0.86
4	−2.96	−0.05
5	−3.02	0.58

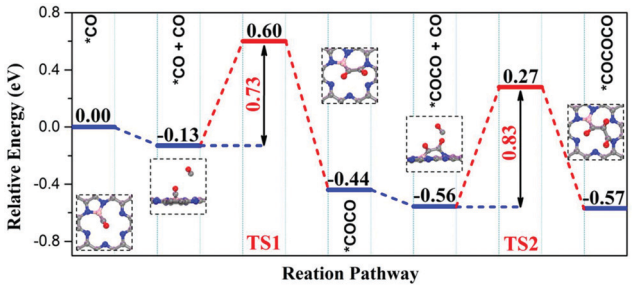

Fig. 3 The detailed energy profile of C–C coupling for two and three CO molecules on B/C_2N, in which * represents the chemisorption state of the first CO on the B site.

orating B atom always accepts electrons and acts as the Lewis acid, while the host N atom binding with the subsequent approaching CO molecules always donates electrons and serves as the Lewis base, based on Hirshfeld population analysis (see Table S2†). As confirmed by the adsorption energy and free energy calculations (see Table 1), the decorating B atom (electron acceptor) strongly captures the first CO molecule; meanwhile the host N atoms (electron donors) push the approaching CO molecules toward the foregoing adsorbed CO molecule or the already formed carbon skeleton, thus promoting the C–C coupling. This highly resembles the pull–push effect observed in borane, boron-metal cation, and B doped BP for the N≡N bond activation.[47–49] Therefore, we believe that the decorating B atom and the host N atoms of the B/C_2N complex do act as the Lewis acid and base, respectively, forming the B–N FLPs with the so-called pull–push function and thus facilitating the multi-CO coupling.

Considering the spontaneous occurrence for C–C coupling on B/C_2N, it is reasonable to believe that the hydrogenation of CO on the B/C_2N complex prefers to start from the spontaneously formed CO dimer or trimer rather than from an isolated CO, which triggers the CO reduction reaction to produce C_2 and C_3 chemicals with the help of B–N FLPs. Fig. 4 summarizes the most energetically favorable reaction pathway (with the lowest positive free energy change between any two elementary steps) towards the formation of ethylene/propylene (C_2H_4/C_3H_6), together with the atomic structures of the corresponding reaction intermediates. As shown in Fig. 4a, reducing the CO dimer to C_2H_4 follows the following reaction path: *COCO → *COHCO → *COHCOH → *COHCHOH → *COHCH → *$COHCH_2$ → *$CHOHCH_2$ → *$CHCH_2$ → *CH_2CH_2. Along this path, the formation of *COHCOH species with the largest positive free energy change (0.22 eV) is the potential-determining step during this process. As for the reduction of the CO trimer, the reduction process proceeds with three O atoms sequentially removed (see Fig. 4b). After removing the 2nd O atom, the center C atom of the CO trimer attaches its nearest N atom, forming a C–N bond. After the last hydrogenation step, the distal C atom bonding with three H atoms lifts up from the B/C_2N basal plane. In this case, the formation of *CH_2CHCHO species is the potential-determining step with a free energy increase of 0.22 eV. Note that the total decreases (4.15 and 5.09 eV) of the Gibbs free energy from the beginning to the end of the hydrogenation for CO dimer and trimer reduction are much larger than the energy costs (2.49 and 2.12 eV) to form gaseous C_2H_4 and C_3H_6 molecules, which indicates an energetically feasible process to release the final products (C_2H_4 and C_3H_6) from the B/C_2N substrate. Energetically, the reduction of the CO dimer and trimer prefers to produce ethylene and propylene, respectively, based on our DFT calculations. However, we cannot exclude the production of other possible oxygenated organics.

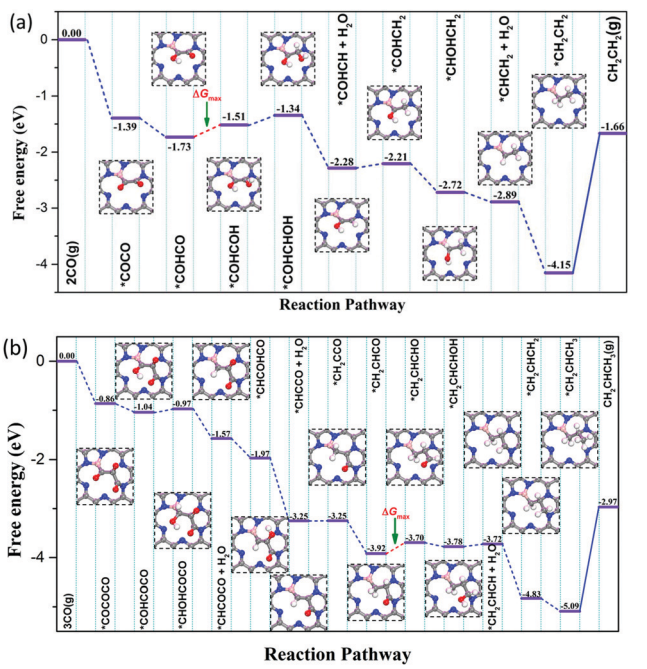

Fig. 4 Gibbs free energy diagrams of CO reduction to (a) C_2H_4 and (b) C_3H_6 at a potential of 0 V. The corresponding atomic structures of relevant reaction intermediates are also given.

Catalytic selectivity towards CO reduction to multi-carbon chemicals

In the above analyses, we theoretically demonstrated the high catalytic activity of the B/C_2N complex towards the reduction of the CO dimer or trimer. However, the adsorbed single CO molecules may also be reduced to other C_1 chemicals such as CH_4 and CH_3OH on the B/C_2N surface, which may affect the selectivity towards the production of C_n chemicals. Thus, we examined the selectivity towards multi-carbon chemicals.

Encouragingly, according to our DFT computations, producing the C_1 chemicals (CH_4 and CH_3OH) from CO reduction has to overcome large free energy barriers (1.85 and 1.80 eV for CH_4 and CH_3OH, respectively; see Fig. S4 in the ESI†). Such high free energy barriers are due to the strong bonding between the decorated B atom and the relevant intermediates during the CO reduction, which severely hinders the formation of saturated hydrocarbons or their oxygenated derivatives.

Significantly, extremely low energy costs (0.22 eV) are needed to be overcome to reduce the CO dimer and trimer to C_2H_4 and C_3H_6, respectively, implying a high catalytic efficiency of the B/C_2N catalyst for CO reduction to C_n chemicals due to the presence of the B–N FLPs. Note that the energy cost (0.22 eV) of reducing the CO dimer to C_2H_4 is identical to that (0.22 eV) of reducing the CO trimer to C_3H_6, giving rise to a mixture of gaseous C_2H_4 and C_3H_6 in the final products, which can be effectively separated by an industrially mature cryogenic distillation method or newly proposed zeolitic imidazolate frameworks.[50]

As a major side reaction of CO reduction, the hydrogen evolution reaction (HER) on our proposed catalyst was also examined by computing its corresponding free energy profile,[51–53] and three active sites (labelled B, N_1, and N_2,

respectively, see Fig. S5 in the ESI†) were considered. Our simulations demonstrated that the HER process on the three sites is hindered by the Heyrovsky step ($H^* + H^+ + e^- \rightarrow H_2$) with the free energy barriers of 2.27, 0.51 and 0.68 eV, respectively, which are much larger than that of CO reduction to C_2H_4 and C_3H_6 (0.22 eV, Fig. 4a and b). Thus, B/C_2N was predicted to exhibit outstanding catalytic selectivity for CO reduction compared to the HER.

In addition, we note that Cao *et al.* proposed the ultra-high catalytic activity of two B atom embedded C_2N nanosheets (B_2/C_2N) for the nitrogen reduction reaction, which is attributed to the synergetic effects of two B atoms.[54] Thus, we expected that the C_{2+} products could also be generated on B_2/C_2N due to the high chemical reactivity of two B atoms. However, the corresponding catalytic pathways will be greatly complicated compared to that on B/C_2N, in which the two B atoms and their around N atoms could be the active sites for CO reduction reactions rather than a mere frustrated Lewis pairs-based catalyst that is composed of one B and host N atoms. Some related computations are being performed and are thus not considered in the present work.

Catalytic CO reduction driven by visible light adsorption

Note that all the above results and discussion on the catalytic activity of B/C_2N to reduce CO to C_n chemicals (C_2 and C_3) are based on the well-known proton-coupled electron transfer electrocatalytic reaction mechanism. Actually, the pristine C_2N is also a metal-free semiconducting photocatalyst with excellent visible light adsorption due to its moderate bandgap.[55–57] Therefore, we further studied the electronic structure of the B/C_2N complex to check its possibility as a metal-free photocatalyst for CO reduction.

Fig. 5a–c present the calculated band structures and light absorption spectra of the monolayer C_2N and B/C_2N, respectively. As shown in Fig. 5a, the pristine C_2N shows a direct bandgap of 2.46 eV, which is consistent with previous reports.[55–57] After decorating the B atom, the bandgap of the B/C_2N complex decreases to 1.20 eV (see Fig. 5b), which further extends its absorption range even into the infrared region (see Fig. 5c). Therefore, the as-designed B/C_2N shows a wider light absorption range than the pristine C_2N, implying its better photocatalytic performance.

More importantly, as shown in Fig. 5d, though slightly lower than that of pristine C_2N due to B atom decoration, the conduction band minimum (CBM) level of B/C_2N still lies about 0.61 and 0.65 eV higher than the calculated reduction potentials of CO/C_2H_4 (0.17 V *vs.* NHE) and CO/C_3H_6 (0.21 V *vs.* NHE), respectively. Therefore, the photoexcited electrons of B/C_2N remain strong enough driving force to fulfill the CO reduction to C_2 and C_3 chemicals, considering the extremely low free energy barrier (0.22 eV) for the potential-determining step to produce both C_2 and C_3 chemicals from CO reduction. All these results clearly demonstrate that our designed B/C_2N complex should act as a highly efficient photocatalyst for CO

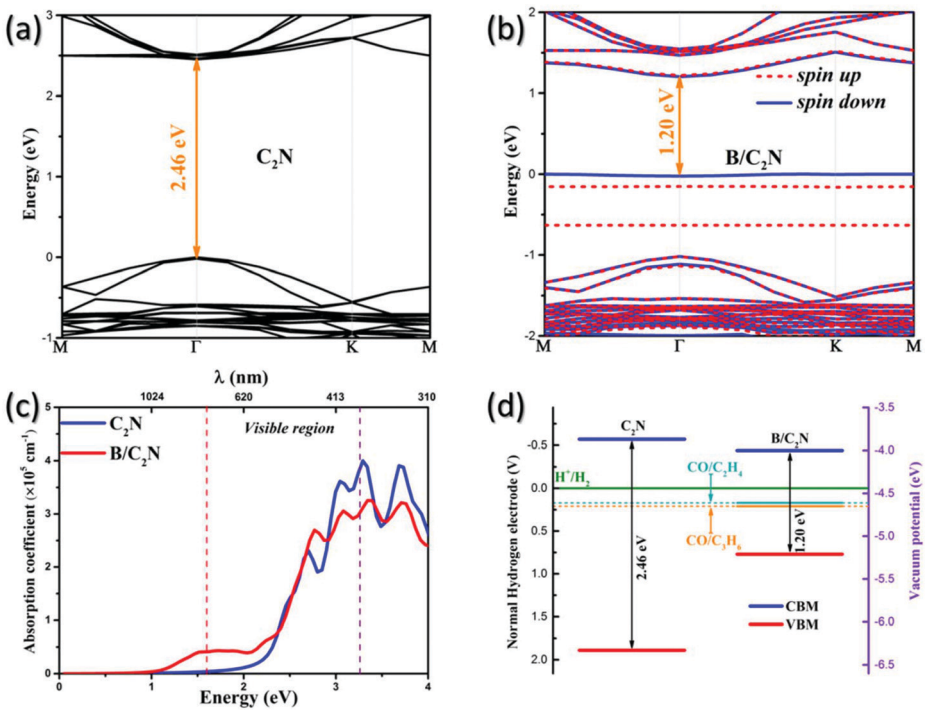

Fig. 5 Band structures of (a) pristine C_2N layer and (b) B/C_2N complex, in which the Fermi levels are set to zero. (c) The calculated light absorption spectra of the pristine C_2N layer and B/C_2N complex, where the visible light range is highlighted between the red and the violet dashed lines. (d) Calculated band edge positions of the pristine C_2N layer and B/C_2N complex. For comparison, the calculated reduction potentials of CO/C_2H_4 and CO/C_3H_6 with respect to the vacuum level as well as NHE are also given.

reduction to C_n chemicals under visible and even infrared light irradiation.

3. Conclusion

In summary, we have designed a frustrated Lewis pairs photocatalyst for the reduction of CO to high value-added multi-carbon chemicals (C_2H_4/C_3H_6) by decorating single B atom on the monolayer C_2N (*i.e.*, B/C_2N). Free energy calculations have clearly revealed that the B/C_2N catalyst can efficiently convert CO into C_2H_4 and C_3H_6 both with the largest free energy increase of 0.22 eV, due to the presence of B–N FLPs in the B/C_2N complex with the pull–push function. Electronic structure calculations indicated that the newly designed B/C_2N complex possesses excellent visible light and even infrared adsorption with a suitable band position, rendering it an ideal photocatalyst for CO reduction to multi-carbon chemicals under visible and even infrared light irradiation. This study not only identified the B/C_2N monolayer as a very promising metal-free photocatalyst for CO reduction to C_n chemicals, which has substantial economic benefits and a significant effect on the long-term application of CO_2 reduction, but also calls for much effort in developing new concepts in modern catalyst design.

4. Computational details

The spin-polarized DFT calculations were performed by using the Vienna Ab Initio Simulation Package (VASP).[58] The generalized gradient approximation (GGA) combined with the Perdew–Burke–Ernzerhof (PBE) functional was employed to describe the exchange–correlation term. The electron-ion interactions were described by the projector augmented wave (PAW) method.[59,60] All geometries were fully optimized with a plane wave energy cutoff of 500 eV and the convergence criterion for the residual force and energy was set to 0.03 eV $Å^{-1}$ and 10^{-5} eV, respectively. We used the empirical correction in Grimme's method (DFT+D3) to describe van der Waals interactions.[61]

The B/C_2N catalyst was constructed by introducing one B atom into a 2 × 2 × 1 supercell of the C_2N monolayer. The vacuum space was set to 15 Å in the *z* direction, which was enough to negligible interactions between periodic units. A 3 × 3 × 1 Monkhorst–Pack *k*-point mesh was used to sample the Brillouin zone. The band structures and light adsorption spectra were calculated by using the hybrid functionals based on the Heyd–Scuseria–Ernzerhof (HSE06) method.[62] The climbing image nudged elastic band (CI-NEB) method was used to calculate the minimum energy path and search the reaction saddle point.[63] *Ab initio* molecular dynamics (AIMD) simulations were performed in the canonical ensemble (NVT) using a Nose–Hoover thermostat to evaluate the thermodynamic stability of the B/C_2N catalyst.[64,65] The phonon band structure was computed using the density functional perturbation theory (DFPT)[66] as implemented in Phonopy package.[67] Hirshfeld population analysis[68] was performed using the PBE functional with a DNP basis set using the DMol^3 program.[69] Other computational details including calculation methods of adsorption energy, free energy and reduction potential can be found in the ESI.†

Conflicts of interest

The authors declare no competing financial interest.

Acknowledgements

This work was financially supported in China by the National Natural Science Foundation of China (NSFC No. 51972312, 51472249) and the Natural Science Funds for Distinguished Young Scholar of Heilongjiang Province (No. JC2018004) and in USA by the NSF-CREST Center for Innovation, Research and Education in Environmental Nanotechnology (CIRE2N) (Grant Number HRD-1736093). The theoretical calculations in this work were performed on TianHe-1(A) at the National Supercomputer Center in Tianjin and Tianhe-2 at the National Supercomputer Center in Guangzhou.

References

1 Y. Chen, C. W. Li and M. W. Kanan, *J. Am. Chem. Soc.*, 2012, **134**, 19969–19972.
2 D. Gao, H. Zhou, J. Wang, S. Miao, F. Yang, G. Wang, J. Wang and X. Bao, *J. Am. Chem. Soc.*, 2015, **137**, 4288–4291.
3 S. Gao, Y. Lin, X. Jiao, Y. Sun, Q. Luo, W. Zhang, D. Li, J. Yang and Y. Xie, *Nature*, 2016, **529**, 68.
4 Y. Jiao, Y. Zheng, P. Chen, M. Jaroniec and S.-Z. Qiao, *J. Am. Chem. Soc.*, 2017, **139**, 18093–18100.
5 J. Jiao, R. Lin, S. Liu, W.-C. Cheong, C. Zhang, Z. Chen, Y. Pan, J. Tang, K. Wu and S.-F. Hung, *Nat. Chem.*, 2019, **11**, 222–228.
6 C. Kim, H. S. Jeon, T. Eom, M. S. Jee, H. Kim, C. M. Friend, B. K. Min and Y. J. Hwang, *J. Am. Chem. Soc.*, 2015, **137**, 13844–13850.
7 D. Kim, J. Resasco, Y. Yu, A. M. Asiri and P. Yang, *Nat. Commun.*, 2014, **5**, 4948.
8 S. Rasul, D. Anjum, H. A. Jedidi, Y. Minenkov, L. Cavallo and K. Takanabe, *Angew. Chem., Int. Ed.*, 2015, **54**, 2146–2150.
9 C. Shan, E. T. Martin, D. G. Peters and J. M. Zaleski, *Chem. Mater.*, 2017, **29**, 6030–6043.
10 S. Zhang, P. Kang and T. J. Meyer, *J. Am. Chem. Soc.*, 2014, **136**, 1734–1737.
11 S. Zhao, R. Jin and R. Jin, *ACS Energy Lett.*, 2018, **3**, 452–462.
12 W. Zhu, L. Zhang, P. Yang, C. Hu, H. Dong, Z.-J. Zhao, R. Mu and J. Gong, *ACS Energy Lett.*, 2018, **3**, 2144–2149.

13 M. Asadi, K. Kim, C. Liu, A. V. Addepalli, P. Abbasi, P. Yasaei, P. Phillips, A. Behranginia, J. M. Cerrato and R. Haasch, *Science*, 2016, **353**, 467–470.
14 M. Asadi, B. Kumar, A. Behranginia, B. A. Rosen, A. Baskin, N. Repnin, D. Pisasale, P. Phillips, W. Zhu and R. Haasch, *Nat. Commun.*, 2014, **5**, 4470.
15 I. Hod, M. D. Sampson, P. Deria, C. P. Kubiak, O. K. Farha and J. T. Hupp, *ACS Catal.*, 2015, **5**, 6302–6309.
16 N. Kornienko, Y. Zhao, C. S. Kley, C. Zhu, D. Kim, S. Lin, C. J. Chang, O. M. Yaghi and P. Yang, *J. Am. Chem. Soc.*, 2015, **137**, 14129–14135.
17 S. Lin, C. S. Diercks, Y.-B. Zhang, N. Kornienko, E. M. Nichols, Y. Zhao, A. R. Paris, D. Kim, P. Yang and O. M. Yaghi, *Science*, 2015, **349**, 1208–1213.
18 S. Liu, H. Yang, X. Huang, L. Liu, W. Cai, J. Gao, X. Li, T. Zhang, Y. Huang and B. Liu, *Adv. Funct. Mater.*, 2018, **28**, 1800499.
19 P. P. Sharma, J. Wu, R. M. Yadav, M. Liu, C. J. Wright, C. S. Tiwary, B. I. Yakobson, J. Lou, P. M. Ajayan and X. D. Zhou, *Angew. Chem., Int. Ed.*, 2015, **54**, 13701–13705.
20 J. Wu, M. Liu, P. P. Sharma, R. M. Yadav, L. Ma, Y. Yang, X. Zou, X.-D. Zhou, R. Vajtai and B. I. Yakobson, *Nano Lett.*, 2015, **16**, 466–470.
21 J. Xu, Y. Kan, R. Huang, B. Zhang, B. Wang, K. H. Wu, Y. Lin, X. Sun, Q. Li and G. Centi, *ChemSusChem*, 2016, **9**, 1085–1089.
22 Z. Gu, N. Yang, P. Han, M. Kuang, B. Mei, Z. Jiang, J. Zhong, L. Li and G. Zheng, *Small Methods*, 2018, **3**, 1800449.
23 M. Jouny, W. Luc and F. Jiao, *Nat. Catal.*, 2018, **1**, 748–755.
24 K. P. Kuhl, E. R. Cave, D. N. Abram and T. F. Jaramillo, *Energy Environ. Sci.*, 2012, **5**, 7050–7059.
25 Y. Liu, Y. Zhang, K. Cheng, X. Quan, X. Fan, Y. Su, S. Chen, H. Zhao, Y. Zhang and H. Yu, *Angew. Chem., Int. Ed.*, 2017, **56**, 15607–15611.
26 J. Wu, S. Ma, J. Sun, J. I. Gold, C. Tiwary, B. Kim, L. Zhu, N. Chopra, I. N. Odeh and R. Vajtai, *Nat. Commun.*, 2016, **7**, 13869.
27 A. Bagger, L. Arnarson, M. H. Hansen, E. Spohr and J. Rossmeisl, *J. Am. Chem. Soc.*, 2019, **141**, 1506–1514.
28 Y. Pang, J. Li, Z. Wang, C.-S. Tan, P.-L. Hsieh, T.-T. Zhuang, Z.-Q. Liang, C. Zou, X. Wang and P. De Luna, *Nat. Catal.*, 2019, **2**, 251–258.
29 Y. Wang, A. Kostenko, T. J. Hadlington, M.-P. Luecke, S. Yao and M. Driess, *J. Am. Chem. Soc.*, 2018, **141**, 626–634.
30 G. C. Welch, R. R. San Juan, J. D. Masuda and D. W. Stephan, *Science*, 2006, **314**, 1124–1126.
31 C. M. Mömming, E. Otten, G. Kehr, R. Fröhlich, S. Grimme, D. W. Stephan and G. Erker, *Angew. Chem., Int. Ed.*, 2009, **48**, 6643–6646.
32 M. Sajid, L. M. Elmer, C. Rosorius, C. G. Daniliuc, S. Grimme, G. Kehr and G. Erker, *Angew. Chem., Int. Ed.*, 2013, **52**, 2243–2246.
33 D. W. Stephan and G. Erker, *Chem. Sci.*, 2014, **5**, 2625–2641.
34 D. W. Stephan and G. Erker, *Angew. Chem., Int. Ed.*, 2015, **54**, 6400–6441.
35 A. Berkefeld, W. E. Piers and M. Parvez, *J. Am. Chem. Soc.*, 2010, **132**, 10660–10661.
36 H. Braunschweig, R. D. Dewhurst, F. Hupp, M. Nutz, K. Radacki, C. W. Tate, A. Vargas and Q. Ye, *Nature*, 2015, **522**, 327–330.
37 R. Dobrovetsky and D. W. Stephan, *J. Am. Chem. Soc.*, 2013, **135**, 4974–4977.
38 C. Ling, X. Niu, Q. Li, A. Du and J. Wang, *J. Am. Chem. Soc.*, 2018, **140**, 14161–14168.
39 H. Wang, L. Wu, Z. Lin and Z. Xie, *Angew. Chem., Int. Ed.*, 2018, **57**, 8708–8713.
40 H. Zhang, Z. Cao, W. Wu and Y. Mo, *Angew. Chem., Int. Ed.*, 2018, **57**, 13076–13081.
41 Z. W. Chen, J. M. Yan and Q. Jiang, *Small Methods*, 2018, **3**, 1800291.
42 X. Li, W. Zhong, P. Cui, J. Li and J. Jiang, *J. Phys. Chem. Lett.*, 2016, **7**, 1750–1755.
43 X. Zhang, A. Chen, Z. Zhang, M. Jiao and Z. Zhou, *J. Mater. Chem. A*, 2018, **6**, 11446–11452.
44 F. Calle-Vallejo and M. T. Koper, *Angew. Chem., Int. Ed.*, 2013, **52**, 7282–7285.
45 Y. Song, W. Chen, C. Zhao, S. Li, W. Wei and Y. Sun, *Angew. Chem.*, 2017, **129**, 10980–10984.
46 J. H. Montoya, A. A. Peterson and J. K. Nørskov, *ChemCatChem*, 2013, **5**, 737–742.
47 J. B. Geri, J. P. Shanahan and N. K. Szymczak, *J. Am. Chem. Soc.*, 2017, **139**, 5952–5956.
48 A. J. Ruddy, D. M. Ould, P. D. Newman and R. L. Melen, *Dalton Trans.*, 2018, **47**, 10377–10381.
49 L. Shi, Q. Li, C. Ling, Y. Zhang, Y. Ouyang, X. Bai and J. Wang, *J. Mater. Chem. A*, 2019, **7**, 4865–4871.
50 Y. Pan and Z. Lai, *Chem. Commun.*, 2011, **47**, 10275–10277.
51 A. Vasileff, Y. Zheng and S. Z. Qiao, *Adv. Energy Mater.*, 2017, **7**, 1700759.
52 Z. Chen, J. Zhao, C. R. Cabrera and Z. Chen, *Small Methods*, 2018, **3**, 1800368.
53 Z. Chen, J. Zhao, L. Yin and Z. Chen, *J. Mater. Chem. A*, 2019, **7**, 13284–13292.
54 Y. Cao, S. Deng, Q. Fang, X. Sun, C. Zhao, J. Zheng, Y. Gao, H. Zhuo, Y. Li, Z. Yao, Z. Wei, X. Zhong, G. Zhuang and J. Wang, *Nanotechnology*, 2019, **30**, 335403.
55 M. Ashwin Kishore and P. Ravindran, *J. Phys. Chem. C*, 2017, **121**, 22216–22224.
56 M. A. Kishore and P. Ravindran, *ChemPhysChem*, 2017, **18**, 1526–1532.
57 R. Kumar, D. Das and A. K. Singh, *J. Catal.*, 2018, **359**, 143–150.
58 G. Kresse and J. Furthmüller, *Phys. Rev. B: Condens. Matter Mater. Phys.*, 1996, **54**, 11169.
59 P. Blöchl, *Phys. Rev. B: Condens. Matter Mater. Phys.*, 1994, **50**, 17953.
60 J. P. Perdew, K. Burke and M. Ernzerhof, *Phys. Rev. Lett.*, 1996, **77**, 3865.
61 S. Grimme and L. Goerigk, *Phys. Chem. Chem. Phys.*, 2011, **13**, 6670–6688.

62 J. Heyd and G. E. Scuseria, *J. Chem. Phys.*, 2003, **118**, 8207–8215.
63 G. Henkelman, B. P. Uberuaga and H. Jónsson, *J. Chem. Phys.*, 2000, **113**, 9901–9904.
64 G. Bussi, D. Donadio and M. Parrinello, *J. Chem. Phys.*, 2007, **126**, 014101.
65 S. Nosé, *J. Chem. Phys.*, 1984, **81**, 511–519.
66 S. Baroni, S. de Gironcoli, A. Dal Corso and P. Gianozzi, *Rev. Mod. Phys.*, 2001, **73**, 515–562.
67 A. Togo, F. Oba and I. Tanaka, *Phys. Rev. B: Condens. Matter Mater. Phys.*, 2008, **78**, 134106.
68 F. L. Hirshfeld, *Theor. Chim. Acta*, 1997, **44**, 129–138.
69 B. Delley, *J. Chem. Phys.*, 1990, **92**, 508–517.